AIP | Applied Physics Letters

Dynamic formation of ring-shaped patterns of colloidal particles in microfluidic systems

David S. W. Lim, J. Patrick Shelby, Jason S. Kuo, and Daniel T. Chiu

Citation: Applied Physics Letters **83**, 1145 (2003); doi: 10.1063/1.1600532
View online: http://dx.doi.org/10.1063/1.1600532
View Table of Contents: http://scitation.aip.org/content/aip/journal/apl/83/6?ver=pdfcov
Published by the AIP Publishing

Dynamic formation of ring-shaped patterns of colloidal particles in microfluidic systems

David S. W. Lim, J. Patrick Shelby, Jason S. Kuo, and Daniel T. Chiu[a)]
Department of Chemistry, University of Washington, Seattle, Washington 98195-1700

(Received 23 April 2003; accepted 11 June 2003)

This letter reports the formation of patterns of micrometer-sized beads within the steady-state recirculation flow of a microvortex generated in a microfluidic system. The mechanism by which these patterns form relies on a delicate balance between the centrifugal and displacement forces experienced by the recirculating particles with a lift force exerted on the particles near the solid boundary of the microcavity. Our observation was made possible by the small dimensions of the microchannels we used and by the presence of steep velocity gradients unique to microfluidic devices. © *2003 American Institute of Physics.* [DOI: 10.1063/1.1600532]

The use of colloidal particles (e.g., microbeads) in a microfluidic system is of central importance for many emerging bioanalytical and biotechnological applications. With the advent of microfluidics,[1–3] many of these bead-based platforms are being implemented in a lab-on-a-chip format.[4] This letter characterizes the behavior of beads in microfluidic systems, and reports the dynamic formation of patterns of beads in a steady-state recirculation flow.

Figure 1(a) depicts the microchannel system used in our experiments, which consists of a 30-μm×30-μm straight channel connected with a diamond-shaped cavity. The channels were fabricated in polydimethylsiloxane (PDMS) using two-step photolithography and replica molding.[5] PDMS molds were irreversibly sealed to glass cover slips after exposure to oxygen plasma. Figures 1(b)–1(e) were imaged in fluorescence using monodisperse 1-μm fluorescent polystyrene beads in water, present at a volume fraction of $\phi \sim 10^{-5}$. At a flow rate of 5 m/s in the 30-μm channel, the recirculating fluorescent microbeads were distributed throughout the microchamber [Fig. 1(b)]. When the flow rate was increased to 9 m/s [Fig. 1(c)], the recirculating beads collapsed to form a bright closed ring with a diameter of ~18 μm. The ring expanded to ~29 μm in diameter at 17 m/s [Fig. 1(d)]. At even higher flow rates [e.g., 45 m/s in Fig. 1(e)], the ring disappeared and the chamber was cleared of beads. The Re numbers at the opening of the microcavity in Figs. 1(b)–1(e) are ~42, 61, 104, and 245, correspondingly. At the velocity in which ring formation occurs, the beads appear to get trapped in the cavity [Figs. 1(c) and 1(d)], but at high velocities [Fig. 1(e)], the beads are forced out of the cavity due to excess centrifugal accelerations. We have observed this dynamic ring formation under a wide range of conditions, including different sizes of beads in solutions of various density and viscosity. Ring formation became less reproducible as the diameter of the bead decreases.

Because the concentrations of beads we used are low ($\phi \sim 10^{-7}$ to 10^{-5}), the particle–particle interaction is weak and the motion of the particles is dominated by their interactions with the fluid. To characterize fluid motion inside the microcavity, we profiled the local fluid velocity using caged fluorescein in the absence of particles.[6] Figures 2(a) and 2(b) are experimental measurements showing the velocity profiles along the dotted lines. The linear velocity approaches zero at the center of rotation, similar to a solid-body rotation. No-

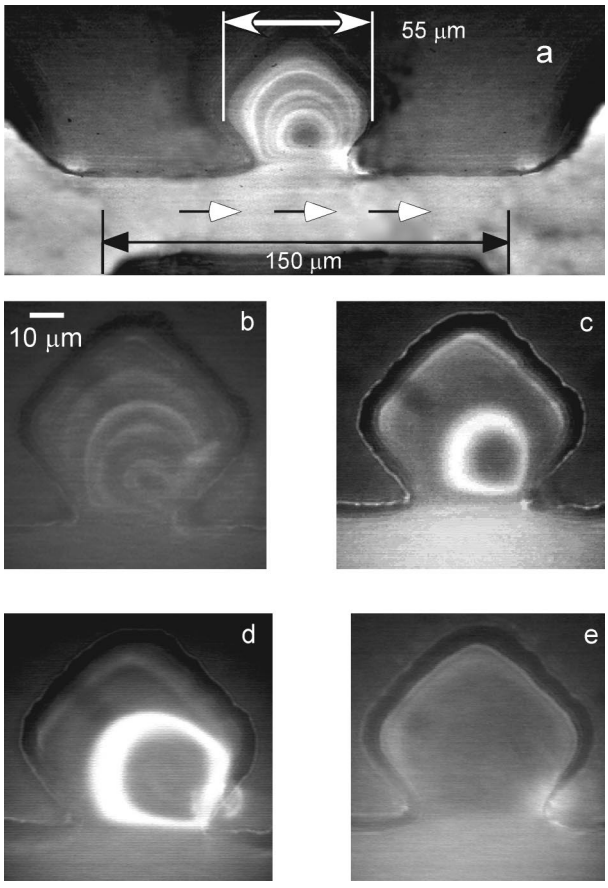

FIG. 1. (a) Fluorescence micrograph showing the layout of the microchannel used in our experiments. To prevent the buildup of back pressure, the 150-μm-long channel (which is 30-μm by 30-μm in cross section) is connected to a large channel having a cross section of 250-μm by 250-μm. The fluorescence observed in the channel and cavity is caused by the presence of 1-μm fluorescent polystyrene beads flowing through the channel. (b)–(e) show the formation of patterns of recirculating 1-μm polystyrene beads (density ~1.05 g/cm^3) in water (volume fraction, $\phi \sim 10^{-5}$), as a function of average flow rate in the 30-μm-wide straight channel, (b) 5 m/s; (c) 9 m/s; (d) 17 m/s; and (e) 45 m/s.

a)Author to whom correspondence should be addressed; electronic mail: chiu@chem.washington.edu

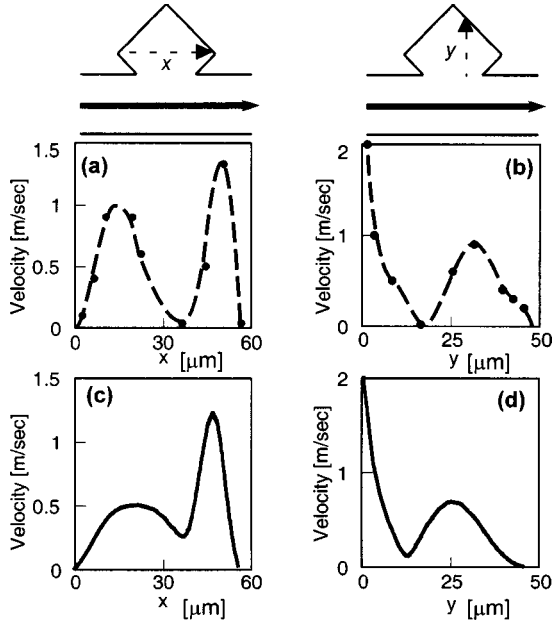

FIG. 2. (a) and (b) are experimental measurements of the velocity profiles inside the microcavity in the absence of beads and at an average flow rate of 5 m/s in the 30-μm wide channel. (c) and (d) are the simulated velocity profiles under identical conditions as those shown in (a) and (b).

slip imposed at the wall of the microchamber forces the fluid velocity to approach zero at the fluid–solid interface. The velocity distribution along the x direction [Fig. 2(a)] is asymmetric because of the considerably higher pressure present at the downstream (right corner) edge of the cavity opening [Fig. 2(b)], which is caused by the deceleration of the fluid element as it enters the cavity from the 30-μm channel. The rapid decrease in flow velocity at the opening along the y direction [Fig. 2(b)] is consistent with the transport of momentum from the straight channel into the microchamber. The experimental measurements [Figs. 2(a) and 2(b)] compare well with our simulated velocity profiles [Figs. 2(c) and 2(d)], which were performed under identical channel geometries and flow rates used in our experiments [Figs. 2(a) and 2(b)].

To understand the mechanism behind this dynamic formation of rings of microbeads, we used a force-balance approach. In a dilute suspension system ($\phi \sim 10^{-7}$ to 10^{-5}) where interparticle interactions are negligible, particles can be considered as isolated entities and the forces exerted on them are predominantly hydrodynamic. For a single bead to follow a stable circular trajectory in our system, there are three dominant forces, which originate from (i) centrifugal acceleration (centr), (ii) fluid displacement (disp), and (iii) hydrodynamic lift. Although there also exists a Stokes drag force, its magnitude is negligible in comparison with these three forces. To form a stable recirculating ring of beads, these three forces must be balanced at the radial location of the ring:

$$F_{\text{centr}} + F_{\text{disp}} + F_{\text{lift}} \approx 0. \tag{1}$$

The centrifugal force (F_{centr}) is caused by the bead traveling in a circular path at high frequency and in the particle frame, it is simply

$$F_{\text{centr}} = m_p \nu_p^2 / r, \tag{2}$$

where m_p and ν_p are, respectively, the mass and linear tangential velocity of the particle, and r is the radius of the ring. We estimate F_{centr} to be $\sim$200 pN using the experimental conditions of Fig. 1(c) (9 m/s in the 30-μm channel).

As a particle, driven by F_{centr}, travels through solution, it must displace a corresponding volume of fluid. If the pressure acting on the particle by the fluid is approximately linear as a function of radius across the length scale of the particle [i.e., $\partial p/\partial r \approx$constant in Eq. (3)], as is the case in traditional centrifugation performed in a test tube, this force (F_{disp}) can be accounted for by using the effective density of the particle (i.e., $\rho_p - \rho_f$) in the calculation of F_{centr}. If the pressure is nonlinear over the diameter of the particle (i.e., $\partial p/\partial r \neq$constant), as in our system, F_{disp} can be calculated in the particle frame from

$$F_{\text{disp}} = \int\int\int (\partial p/\partial r) dV = \int\int\int \rho_f \nu_\theta^2 / r \, dV, \tag{3}$$

where $\partial p/\partial r$ is the change in pressure along r, ρ_f is the density of the fluid, ν_θ is the azimuthal velocity of the fluid, r is the radial distance from the center of rotation, and the integral is evaluated over the volume of the bead. Using our measured velocity profile [Figs. 2(a) and 2(b)] and with experimental values from Fig. 1(c), $F_{\text{disp}} \sim$140 pN.

The dominant force pushing the bead inward is caused by a hydrodynamic lift (F_{lift}) experienced by the bead as it travels parallel to the boundary of the microcavity. This lift force acts in the direction normal to the wall of the cavity and orthogonal to the trajectory of the bead. The dominant contribution to this hydrodynamic lift is the Saffman lift[7,8] and can be written in its generalized form in the particle frame as

$$F_{\text{lift}} = \rho_f \, a^2 \nu^2 \int\int \sigma \, \mathbf{n} \, dS, \tag{4}$$

which is expressed as the surface integral of the normal stresses of the fluid evaluated over a surface. Here, ρ_f is the density of the fluid, a is the radius of the bead, ν is the characteristic velocity, which is defined as the local velocity of the center of the particle relative to the fluid, σ is the fluid stress, and $\mathbf{n}$ is unit vector normal to the surface. When the velocity of a neutrally buoyant particle is comparable to the velocity of the fluid in a shear flow, however, the characteristic velocity takes the form of $\nu = a\gamma$, where γ is the velocity gradient.

Equation (4) includes contribution from the conventional Saffman force,[8] which describes the hydrodynamic lift in a slow unbounded shear flow, as well as the lateral inertial force exerted on a particle when it is in close contact with the wall under shear flow.[9] The integral in Eq. (4) has to be evaluated numerically but a quadratic form has been derived from the numerical solution[7]

$$\begin{aligned} F_{\text{lift}} = \rho_f \, a^2 \nu^2 [&(1.7716 + 0.216\kappa - 0.792\kappa^2 + 0.4854\kappa^3) \\ &- (0.3297/\kappa + 1.1450 + 2.0840\kappa - 0.9059\kappa^2)\Delta \\ &+ (2.0069 + 1.0575\kappa - 2.4007\kappa^2 + 1.3174\kappa^3)\Delta^2]. \end{aligned} \tag{5}$$

The parameter κ is the ratio of particle radius to the distance between the center of the particle and the wall, and Δ is the

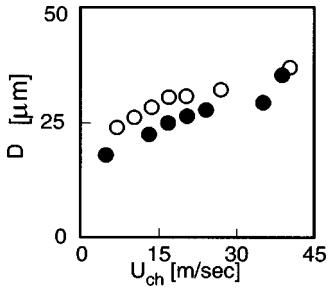

FIG. 3. A plot of ring diameter versus the average flow velocity inside the microchannel. (●) are experimental measurements and (○) are simulated ring diameters using our force-balance model [i.e., from Eqs. (1), (2), (3), and (5)]. Above 45 m/s, no rings were observed because beads were spun out of the cavity due to high F_{centr}.

dimensionless shear. Using Eq. (5) and with $\kappa=0.025$, $\Delta=1$, and $\gamma\sim10^5$ s^{-1} ($\nu=a\gamma$) for our system (i.e., parameters identical to those used for the calculation of F_{centr} and F_{disp}), we estimated F_{lift} to be ~60 pN. F_{lift} becomes especially significant in a microfluidic system in which the characteristic length of the flow is comparable to the particle size; that is, $2a/D$ is approximately $\geqslant0.03$, where a is the radius of the bead and D is the diameter of the ring.

Although preferential migration of particles has been observed previously in simple shear flows,[10,11] the underlying mechanism of migration described in these previous studies, which occurs only at high volume fractions of beads ($\phi\geqslant0.1$), is driven mainly by interparticle interactions, and is fundamentally different from the phenomenon studied in our experiments, where the volume fraction of beads is orders of magnitude lower ($\phi\sim10^{-7}$ to 10^{-5}). In our system, the migration of particles is caused by their interactions with the boundary of our microcavity and the resultant force that arises from the deformation of the velocity profile by the beads near the solid interface.[8,12] This lift force originates from the steep velocity gradient present in the microvortex, which arises because of the high surface-to-volume ratio environment that is unique to microfluidic devices.

Our model is based on a force balance between the outward inertial force ($F_{\text{centr}}-F_{\text{disp}}$) and the inward shear force (F_{lift}) experienced by the beads. This model predicts the diameter of the ring of recirculating beads to increase with the applied inertial force. The diameter of the ring can be estimated by solving the force balance Eqs. [i.e., Eqs. (1), (2), (3), and (5)]. Figure 3 shows a direct comparison of ring diameter versus flow rate between experiments (dark circle) and our model (open circle). The overestimation of the ring diameter in our model is likely caused by the assumption inherent in Eq. (5), because the generalized Saffman lift force [Eq. (5)] was derived using a flat wall. Because the diamond-shaped microcavity in our experiment contains multiple flat walls, the magnitude of the lift force experienced by the particles in our experiment may be greater than predicted by Eq. (5).

The dynamic formation of patterns of recirculating beads described in this letter requires the presence of steep velocity gradients and the high surface-to-volume ratio environment that is characteristic of microfluidic systems. With intense efforts to develop integrated and functional microfluidic devices together with the wide-spread usage of colloidal particles (e.g., microbeads and live cells) in biotechnology, an understanding of the behavior of these particles within environments that are unique to microsystems is essential. The mechanism that underlies bead migration described in this letter, which differs from previous accounts that use very high concentrations of beads, may also be exploited for the separation and concentration of biological particles in analytical applications, such as in flow cytometry.

We are grateful to Prof. J. Michael Schurr for helpful discussions. Two of the authors (D.L. and J.K.) acknowledge partial support from the Joint Institute for Nanoscience funded by the Pacific Northwest National Laboratory (operated by Battelle for the U.S. Department of Energy) and the University of Washington. One author (P.S.) thanks the Center for Nanotechnology at the University of Washington for an IGERT fellowship. This research was partially funded by NIH and NSF, and by starter grants from the Research Corporation and the Dreyfus Foundation.

[1] D. R. Reyes, D. Iossitidis, P. Auroux, and A. Manz, Anal. Chem. **74**, 2623 (2002).
[2] P. Auroux, D. Iossitidis, D. R. Reyes, and A. Manz, Anal. Chem. **74**, 2637 (2002).
[3] G. M. Whitesides and A. D. Stroock, Phys. Today **6**, 42 (2001).
[4] A. Y. Fu, H. P. Chou, C. Spence, F. H. Arnold, and S. R. Quake, Anal. Chem. **74**, 2451 (2002).
[5] J. R. Anderson, D. T. Chiu, R. J. Jackman, O. Cherniavskaya, J. C. McDonald, H. K. Wu, S. H. Whitesides, and G. M. Whitesides, Anal. Chem. **72**, 3158 (2000).
[6] J. P. Shelby and D. T. Chiu, Anal. Chem. **75**, 1387 (2003).
[7] P. Cherukat and J. B. McLaughlin, J. Fluid Mech. **263**, 1 (1994).
[8] P. G. Saffman, J. Fluid Mech. **22**, 385 (1965).
[9] D. Leighton and A. Acrivos, J. Appl. Math. Phys. **36**, 174 (1985).
[10] N. Tetlow, A. L. Graham, M. S. Ingber, S. R. Subia, L. A. Mondy, and S. A. Altobelli, J. Rheol. **42**, 307 (1998).
[11] R. E. Hampton, A. A. Mammoli, A. L. Graham, N. Tetlow, and S. A. Altobelli, J. Rheol. **41**, 621 (1997).
[12] B. P. Ho and L. G. Leal, J. Fluid Mech. **65**, 365 (1974).